

## Axisymmetric and beamlike vibrations of multiwall carbon nanotubes

C. Y. Wang, C. Q. Ru,\* and A. Mioduchowski

*Department of Mechanical Engineering, University of Alberta, Edmonton, Canada T6G 2G8*

(Received 30 December 2004; revised manuscript received 11 April 2005; published 11 August 2005)

Several vibration problems of multiwall carbon nanotubes (MWNTs) are studied in detail based on a multiple-elastic shell model. According to recent data available in the literature, an updated value of bending stiffness for single-wall carbon nanotubes (SWNTs) is suggested, which is in a much better agreement with atomistic model for phonon-dispersion relation of SWNTs. For axisymmetric vibrations (with circumferential wave number  $n=0$ ), it is found that longitudinal ( $L$ ) modes of individual tubes of a MWNT have almost identical frequencies and are usually coupled with each other through Poisson-ratio effect-induced radial ( $R$ ) vibrations and interlayer van der Waals interaction. Especially in the transition zone of  $R$ - and  $L$  modes, the significant Poisson-ratio effect leads to mixed  $R$ - $L$  modes with comparable longitudinal and radial displacements. On the other hand, for beamlike vibrations (with  $n=1$ ), the present multiple-shell model is found to be in good agreement with the multiple-beam model for almost coaxial bending ( $B$ ) modes of large- and small-radius MWNTs and noncoaxial  $B$  modes of small-radius MWNTs (e.g., of the outermost radius less than 2 nm), with relative errors less than 10%. However, for high-order noncoaxial modes of large-radius MWNTs, the relative errors between the two models increase up to 50% in extreme cases due to larger non-beamlike deformation of the cross section while both models give similar overall vibration modes through the entire length of MWNTs. In particular, for lower circumferential wave numbers ( $n=0-10$ ), the lowest frequency always corresponds to the minimum half-axial wave number  $m=1$  for simply supported end conditions. When the wave vector decreases, the lowest frequency decreases and the associated mode shifts from an  $R$  mode with larger  $n$  to a coaxial  $B$  mode with  $n=1$ .

DOI: [10.1103/PhysRevB.72.075414](https://doi.org/10.1103/PhysRevB.72.075414)

PACS number(s): 61.46.+w, 62.25.+g, 68.65.-k

### I. INTRODUCTION

Vibration of carbon nanotube (CNTs) has excited considerable experimental and theoretical studies. The dominant experimental technique has been Raman spectroscopy.<sup>1</sup> As an indirect approach, Raman spectra of CNTs can only be interpreted on the basis of theoretic prediction. Therefore, atomistic models, e.g., zone folding,<sup>2</sup> tight binding,<sup>3</sup> force constant,<sup>4</sup> lattice-dynamical model,<sup>5</sup> and first principles<sup>6</sup> are first employed to simulate vibrational behaviors of CNTs. Since, in many cases, these discrete approaches remain formidable and computationally prohibitive for large-scale atom system like multiwall carbon nanotubes (MWNTs), continuum models, such as elastic beam models,<sup>7,8</sup> elastic shell models,<sup>9-11</sup> and other continuum models<sup>12-16</sup> have been widely used to study phonon-dispersion relations and vibrational modes for CNTs.

Previously, Raman-active radial breathing modes (RBMs) of both SWNTs (Refs. 2-6) and MWNTs (Refs. 17-19) have been studied extensively. These axially uniform axisymmetric modes (with axial half-wave number  $m=0$  and circumferential wave number  $n=0$ ) provide a useful tool to investigate structure-vibrational property relation for CNTs. More recently, other axisymmetric radial ( $R$ ), longitudinal ( $L$ ), and torsional ( $T$ ) modes, which are not necessarily uniform in the axial direction, have also been examined for SWNTs,<sup>14</sup> where strong  $R$ - $L$  coupling is observed as a unique feature for SWNTs of cylindrical symmetry. However, axisymmetric vibrations of MWNTs, as well as general vibration behavior of MWNTs, have not been studied in the literature. On the other hand, beamlike vibrations of MWNTs have been the

topic of numerous recent research. For example, based on a multiple-beam model,<sup>8</sup> beamlike vibrations of MWNTs have been examined for MWNTs of small innermost diameter. It is predicted that the interlayer van der Waals (vdW) interaction results in noncoaxial intertube vibration of MWNTs. This unique phenomenon was later confirmed for DWNTs by a more accurate molecular-structure-mechanics model,<sup>20</sup> although the accuracy and limitations of the multiple-beam model remain unexplored in the literature.

Recently, a multiple-shell model,<sup>21-23</sup> previously used to study buckling behaviors of MWNTs (Refs. 24,25) of up to 20 layers, has been used to study RBMs of MWNTs.<sup>26,27</sup> It is shown that the main features of RBMs observed in experiment and atomistic simulations for MWNTs can be clearly explained by the multiple-shell model and, especially, the RBM frequencies given by the shell model for 2-3 wall CNTs (of the innermost diameter 0.68 to 2.72 nm) are in excellent agreement with molecular dynamics (MD) simulations with relative errors less than 5%.<sup>26</sup> These results suggest that the multiple-shell model has the potential to study complicated vibration behavior of MWNTs, a topic which has not been studied systematically so far and would not easily be studied by other experimental or molecular dynamics methods.

In the present work, an updated bending stiffness ( $D=2$  eV) of SWNTs is suggested based on recent data in the literature, which is in much better agreement with atomistic model for phonon dispersion relations of SWNTs than the previously adopted value ( $D=0.85$  eV) estimated by Yakobson *et al.*<sup>30</sup> based on earlier data of Roberson *et al.*<sup>31</sup> Using the multiple-shell model with  $D=2$  eV, this paper gives a

comprehensive study on axisymmetric modes ( $n=0$ ) of MWNTs, with an emphasis on the unique features of axisymmetric modes for MWNTs and the effect of the Poisson ratio of SWNTs on coupling between  $R$ - and  $L$  modes of MWNTs. Furthermore, the present shell model is employed to study beamlike vibrational ( $n=1$ ) modes of MWNTs and examine the accuracy and applicability of the multiple-beam model.<sup>8</sup> Finally, the lowest frequency and associated modes of MWNTs are studied in detail.

## II. THE MULTIPLE-ELASTIC SHELL MODEL

To study mechanical behaviors of MWNTs, a multiple-elastic shell model<sup>21–23</sup> has been developed, which treats each of the nested tubes of a MWNT as an individual elastic shell coupled with adjacent tubes through normal vdW interaction, while the interlayer friction is negligible. Here, vibration of an elastic shell in the absence of tangential force is described by Flugge dynamic equations.<sup>28,29</sup> Applying Flugge equations to each nested tube of an  $N$ -wall CNT yields  $3N$  equations governing the free vibrations of the  $N$ -wall CNT ( $k=1, 2, \dots, N$ ).

$$\begin{aligned}
& \frac{r_k}{2}(1+\nu)\frac{\partial^2 u_k}{\partial x \partial \theta} + \frac{r_k}{2}(1-\nu)\frac{\partial^2 v_k}{\partial x^2} + \frac{\partial^2 v_k}{\partial \theta^2} - \frac{\partial w_k}{\partial \theta} \\
& + (1-\nu^2)\frac{D}{Ehr_k^2} \left[ \begin{array}{l} \frac{3r_k^2}{2}(1-\nu)\frac{\partial^2 v_k}{\partial x^2} \\ + \frac{r_k^2}{2}(3-\nu)\frac{\partial^3 w_k}{\partial x^2 \partial \theta} \end{array} \right] \\
& = \frac{\rho h}{Eh}(1-\nu^2)r_k^2\frac{\partial^2 v_k}{\partial t^2}, \\
& r_k^2\frac{\partial^2 u_k}{\partial x^2} + \frac{1}{2}(1-\nu)\frac{\partial^2 u_k}{\partial \theta^2} + \frac{r_k}{2}(1+\nu)\frac{\partial^2 v_k}{\partial x \partial \theta} - \nu r_k\frac{\partial w_k}{\partial x} \\
& + (1-\nu^2)\frac{D}{Ehr_k^2} \left[ \begin{array}{l} \frac{1}{2}(1-\nu)\frac{\partial^2 u_k}{\partial \theta^2} \\ + r_k^3\frac{\partial^3 w_k}{\partial x^3} \\ - \frac{r_k}{2}(1-\nu)\frac{\partial^3 w}{\partial x \partial \theta^2} \end{array} \right] \\
& = \frac{\rho h}{Eh}(1-\nu^2)r_k^2\frac{\partial^2 u_k}{\partial t^2}, \\
& \nu r_k\frac{\partial u_k}{\partial x} + \frac{\partial v_k}{\partial \theta} - w_k - (1-\nu^2)\frac{D}{Eh}r_k^2 \cdot \nabla^4 w_k \\
& + (1-\nu^2)\frac{D}{Ehr_k^2} \left[ \begin{array}{l} -r_k^3\frac{\partial^3 u_k}{\partial x^3} + \frac{r_k}{2}(1-\nu)\frac{\partial^3 u_k}{\partial x \partial \theta^2} \\ - \frac{R_k^2}{2}(3-\nu)\frac{\partial^3 v_k}{\partial x^2 \partial \theta} - w_k \\ - 2\frac{\partial^2 w_k}{\partial \theta^2} \end{array} \right] \\
& = \frac{1}{Eh}(1-\nu^2)r_k^2 \left[ \rho h\frac{\partial^2 w_k}{\partial t^2} - p_k \right], \quad (1)
\end{aligned}$$

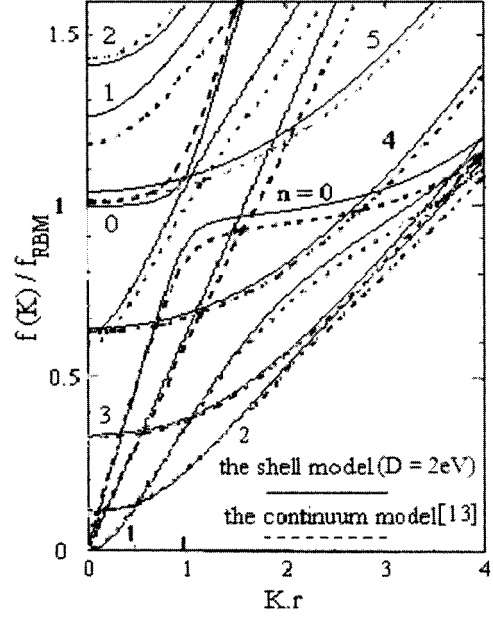


FIG. 1. The comparison between the continuum model (Ref. 13) and the multiple-shell model with  $D=2$  eV for phonon-dispersion relations of SWNT (10, 10). Here,  $K(=m\pi/L)$  is wave vector,  $r$  is the radius of SWNT (10, 10), and  $f_{RBM}$  is RBM frequency of the SWNT.

where  $x$  and  $\theta$  are axial and angular circumferential coordinates,  $t$  is time,  $u_k$ ,  $v_k$ , and  $w_k$  are longitudinal, circumferential, and radial vibration displacements of tube  $k$ , respectively,  $r_k$  is the radius of tube  $k$ , the subscript 1, 2, ..., and  $N$  denote the quantities of the innermost tube 1, its adjacent tube 2, ..., and the outermost tube  $N$ . For each tube (a SWNT),  $D$  is effective bending stiffness,  $Eh$  is in-plane stiffness,  $\rho h$  is mass density per unit lateral area, and  $\nu$  is Poisson ratio. The effective values are  $Eh=360$  J/m<sup>2</sup>,<sup>30</sup>  $\rho h=(2.27$  g/cm<sup>3</sup>) $\times 0.34$  nm, and  $\nu=0.2$ .<sup>24–27</sup> For RBM of a SWNT of radius  $r$ , the present shell model gives the frequency  $230$  cm<sup>-1</sup> (nm/2r), in good agreement with the experimental result of  $224$  cm<sup>-1</sup> (nm/2r).<sup>12,17,26</sup> In addition, excellent agreement<sup>26</sup> between the shell model based on these constant parameters and MD simulation for RBMs (independent of  $D$ ) of MWNTs implies that the possible diameter dependence of these parameters is negligible for diameters down to 0.7 nm. On the other hand, the bending stiffness  $D$  is related to the elastic strain energy per unit area  $U$  by the relationship  $U=D/2r^2$ , where  $r$  is the radius of SWNTs. The value  $D=0.85$  eV, used in our previous work,<sup>24–27</sup> was suggested by Yakobson *et al.*<sup>30</sup> based on Robertson *et al.*'s data<sup>31</sup> published in 1992. However, recent data obtained by *ab initio* calculations yield  $2U \times r^2=4$ – $4.32$  eV (Å<sup>2</sup>/atom) in Ref. 6 (1999),  $3.9$ – $4.32$  eV (Å<sup>2</sup>/atom) in Ref. 32, (2001) and  $4.28$  eV (Å<sup>2</sup>/atom) in Ref. 33 (2002), which suggest an effective value  $D=1.95$ – $2.16$  eV. Indeed, as will be shown later (see Figs. 1 and 2), the updated value  $D=2$  eV for the shell model offers much better fit to an atomistic model<sup>4</sup> than the value  $D=0.85$  eV. Thus, the updated value  $D=2$  eV based on recent data will be used throughout this paper. Here, it should be

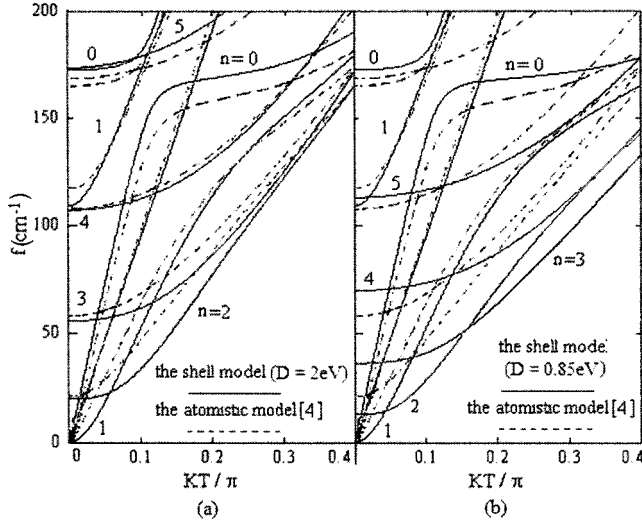


FIG. 2. The comparison between the atomistic model (Ref. 4) and the multiple-shell model with (a)  $D=2$  eV and (b)  $D=0.85$  eV for phonon-dispersion relations of SWNT (10, 10). Here,  $K(=m\pi/L)$  is wave vector and  $T$  represents the shortest repeat distance between two atomic cells along axis of the SWNT.

stated that all related data available in the literature confirm that the possible diameter dependence of bending stiffness  $D$  for SWNTs is negligible for diameters down to 0.7 nm.

Moreover, in view of the multiple-shell model,<sup>21–23</sup> the (inward positive) net radial pressure  $p_k$  on tube  $k$  in Eqs. (1) is given as follows:

$$p_k = c \times (w_{k+1} - w_k) - c \times \frac{r_{k-1}}{r_k} \times (w_k - w_{k-1})$$

$$(k = 2, 3, \dots, N-1),$$

$$p_1 = c \times (w_2 - w_1) \text{ and } p_N = -c \times \frac{r_{N-1}}{r_N} (w_N - w_{N-1}), \quad (2)$$

where  $c$  is the vdW interaction coefficient which depends on the equilibrium interlayer spacing (0.34 nm). In our previous work,<sup>24–27</sup> the value of  $c$  is suggested as

$$c = \frac{320 \times \text{erg/cm}^2}{0.16d^2} \quad (d = 1.42 \times 10^{-8} \text{ cm}). \quad (3)$$

Here, we consider an  $N$ -wall CNT with two ends simply supported. To satisfy the specific boundary conditions, the solutions to Eqs. (1) are given by ( $k=1, 2, \dots, N$ )

$$u_k(x, \theta, t) = U_k \cos \frac{m\pi x}{L} \cos n\theta \times e^{i\omega t},$$

$$v_k(x, \theta, t) = V_k \sin \frac{m\pi x}{L} \sin n\theta \times e^{i\omega t},$$

$$w_k(x, \theta, t) = W_k \sin \frac{m\pi x}{L} \cos n\theta \times e^{i\omega t}, \quad (4)$$

where real numbers  $U_k$ ,  $V_k$ , and  $W_k$  denote the longitudinal, circumferential, and radial displacement amplitudes of tube  $k$ , respectively,  $L$  is the length of the  $N$ -wall CNT,  $\omega$  ( $\omega = 2\pi f$ ,  $f$  is frequency) represents the angular frequency,  $m$  is the axial half-wave number and  $n$  is the circumferential wave number. Substituting Eqs. (2), (3), and (4) into (1) leads to the following  $3N$  equations:

$$M\{(n, m), \omega\}_{3N \times 3N} \begin{bmatrix} U_1 \\ V_1 \\ W_1 \\ \cdots \\ U_N \\ V_N \\ W_N \end{bmatrix} = 0, \quad (5)$$

where  $M_{3N \times 3N}$  is a  $3N \times 3N$  matrix, whose elements are functions of  $(m, n)$ , and  $\omega$ . The condition for existence of nonzero solutions  $U_k$ ,  $V_k$ , and  $W_k$  ( $k=1, 2, \dots, N$ ) is

$$\det M = 0. \quad (6)$$

It is known that the key parameters of free-vibration modes are the circumferential wave number  $n$  and the normalized wave vector  $K \cdot r_N$ , where  $r_N$  is the outermost radius of an  $N$ -wall CNT and  $K$  is wave vector along the tube axis defined by  $K=2\pi/\lambda=m\pi/L$ , with  $\lambda=2L/m$  as axial wavelength. Thus, the normalized wave vector  $K \cdot r_N$   $\{=\pi/[L/(r_N m)]\}$  is inversely proportional to the normalized wavelength  $L/(r_N m)$  (normalized by the outermost diameter  $2r_N$ ). Throughout this paper, our results for MWNTs will be given in terms of  $(Kr_N, n)$ . With given  $K \cdot r_N$  and  $n$ , condition (6) determines  $3N$  frequencies for an  $N$ -wall CNT. Substitution of a frequency into (5) yields amplitude ratios  $U_k/W_N$ ,  $V_k/W_N$ , and  $W_k/W_N$  ( $k=1, 2, \dots, N$ ), defining the associated mode of the  $N$ -wall CNT. Therefore, for each combination of  $(Kr_N, n)$ , an  $N$ -wall CNT has  $3N$  vibration frequencies associated with  $3N$  vibration modes.

To demonstrate the relevance of the elastic shell model for free vibration of CNTs, phonon-dispersion relations are calculated in Figs. 1 and 2 based on Eqs. (1) and (4) for SWNT (10, 10). Here, in order to compare our results with different authors' results,<sup>4,13</sup> frequencies have been given in different units in Figs. 1 and 2. It is seen from Figs. 1 and 2(a) that, overall, the present shell model with  $D=2$  eV is in good agreement with a continuum elastic model<sup>13</sup> and a force-constant model<sup>4</sup> with maximum relative errors usually less than 10%. Particularly, for  $n=1-3$  and smaller normalized wave vector the present shell model with  $D=2$  eV almost coincides with the continuum model,<sup>13</sup> while the two continuum models are a little different from the force constant model.<sup>4</sup> As mentioned in Ref. 13, this discrepancy is probably due to "an inappropriate choice of force-constant value" in Ref. 4. In fact, the phonon dispersion relations of SWNT (10, 10) are also obtained by a lattice-dynamic model and *ab initio* calculation in Refs. 5 and 6, respectively. Different

TABLE I. The data of geometry of four examples of MWNTs.

Example	1	2	3	4
$R_1$ (nm)	5	5	0.65	0.65
Number of layers $N$	2	5	2	5

from Ref. 4, which gives an almost linear frequency- $K$  (wave vector) relation for long-wavelength bending modes ( $n=1$ ), the results of Refs. 5 and 6 show an approximate  $K^2$  dispersion for the long-wavelength bending mode, which favors our results shown in Figs. 1 and 2(a). Since the figures shown in Refs. 5 and 6 are too small for a detailed comparison, the present shell model has been compared to the atomistic model used in Ref. 4 only. On the other hand, it is seen in Fig. 2(b) that the shell model with  $D=0.85$  eV leads to much larger relative errors as compared to the force-constant model, especially for larger  $n$  and the normalized wave vector  $KT/\pi$ , where  $T$  represents the shortest repeat distance between two atomic cells along axis of the SWNT. Here, it should be stated that the previous continuum model<sup>13</sup> and the force-constant model<sup>4</sup> are limited to SWNTs. Indeed, because no detailed experimental or atomistic simulation results are available for phonon-dispersion relation of MWNTs, similar comparison for the present multiple-shell model cannot be made for MWNTs.

In what follows, we shall apply the multiple-shell model with  $D=2$  eV to study axisymmetric and beamlike vibrations of MWNTs. To this end, four examples of MWNTs in Table I are considered, i.e., large-radius MWNTs, examples 1 and 2 with the innermost radius 5 nm, and small-radius MWNTs, examples 3 and 4 with the innermost radius 0.65 nm.

### III. AXISYMMETRIC VIBRATIONS OF MWNTs ( $n=0$ )

In axisymmetric vibration ( $n=0$ ), solution (4) takes the form ( $k=1, 2, \dots, N$ )

$$u_k(x, \theta, t) = U_k \cos \frac{m\pi x}{L} \times e^{i\omega t}$$

$$v_k(x, \theta, t) = 0$$

$$w_k(x, \theta, t) = W_k \sin \frac{m\pi x}{L} \times e^{i\omega t}. \quad (7)$$

With this solution the  $N$  circumferential dynamic equations in Eqs. (1) are satisfied automatically. As a result, the  $3N$  equations in (1) reduce to  $2N$  equations for an  $N$ -wall CNT ( $k=1, 2, \dots, N$ )

$$r_k^2 \frac{\partial^2 u_k}{\partial x^2} - \nu r_k \frac{\partial w_k}{\partial x} + (1 - \nu^2) \frac{D}{Eh} r_k \frac{\partial^3 w_k}{\partial x^3} = \frac{\rho h}{Eh} (1 - \nu^2) r_k^2 \frac{\partial^2 u_k}{\partial t^2},$$

$$\nu r_k \frac{\partial u_k}{\partial x} - w_k - (1 - \nu^2) \frac{D}{Eh} r_k^2 \cdot \frac{\partial^4 w_k}{\partial x^4}$$

$$+ (1 - \nu^2) \frac{D}{Eh r_k^2} \left[ -r_k^3 \frac{\partial^3 u_k}{\partial x^3} \right]$$

$$= \frac{1}{Eh} (1 - \nu^2) r_k^2 \left[ \rho h \frac{\partial^2 w_k}{\partial t^2} - p_k \right]. \quad (8)$$

When the axial wavelength-to-diameter ratio [ $L/(r_N m)$ ] is much larger than 1, i.e., the normalized wave vector  $Kr_N$  is much smaller than 3, the bending stiffness  $D$ -related coupled terms in (8) are negligible. In this case, the axial displacement and radial displacement are decoupled if the Poisson ratio is set to be zero. Hence, the nonzero Poisson ratio plays a crucial role in  $R$ - $L$  coupling. On the other hand, if an  $\theta$ -independent circumferential vibration is considered, one should consider the solution given by<sup>29</sup>

$$u_k(x, \theta, t) = 0,$$

$$v_k(x, \theta, t) = V_k \sin \frac{m\pi x}{L} \times e^{i\omega t},$$

$$w_k(x, \theta, t) = 0. \quad (9)$$

It is readily verified that the following  $N$  uncoupled equations can be derived from (1), for  $N$  uncoupled torsional ( $T$ ) modes ( $k=1, 2, \dots, N$ ):

$$\frac{r_k^2}{2} \times \frac{\partial^2 v_k}{\partial x^2} + (1 - \nu^2) \times \frac{3D}{2Eh} \cdot \frac{\partial^2 v_k}{\partial x^2} = \frac{\rho h}{Eh} (1 + \nu) \times r_k^2 \times \frac{\partial^2 v_k}{\partial t^2}. \quad (10)$$

Here, it should be stated that such decoupled equations are not available for  $\theta$ -dependent circumferential vibration. Obviously, for  $\theta$ -independent pure  $T$  modes of a MWNT, each constituent tube behaves exactly like an isolated SWNT without coupling with adjacent tubes. In particular, the second term is much smaller than the first term on the left-hand side of (10), indicating that  $T$ -mode frequencies will be radius insensitive. Thus,  $T$  modes of MWNTs will not be further discussed in much detail. In the following, we will focus on  $R$ - and  $L$  modes of MWNTs for examples 1–4.

#### A. Axisymmetric radial modes

First, let us consider DWNTs, i.e., examples 1 and 3 of inner radius 5 and 0.65 nm, respectively. When  $n=0$ , frequencies  $R_1$  and  $R_2$  of  $R$  modes, frequencies  $L_1$  and  $L_2$  of  $L$  modes, and frequencies  $T_1$  and  $T_2$  of  $T$  modes are displayed in Figs. 3(a) and 3(b) for examples 1 and 3, respectively. Because MWNTs have a large number of frequencies, it is essential to classify these frequencies into  $L$ ,  $R$ ,  $T$  or coupling  $R$ - $L$  modes based on their amplitude ratios. Thus, it is crucial to calculate the amplitude ratios of vibration mode associated with each frequency. The amplitude ratios associated with  $R$ - and  $L$  modes of examples 1 and 3 are calculated and selectively shown in Fig. 4. In particular, as stated be-

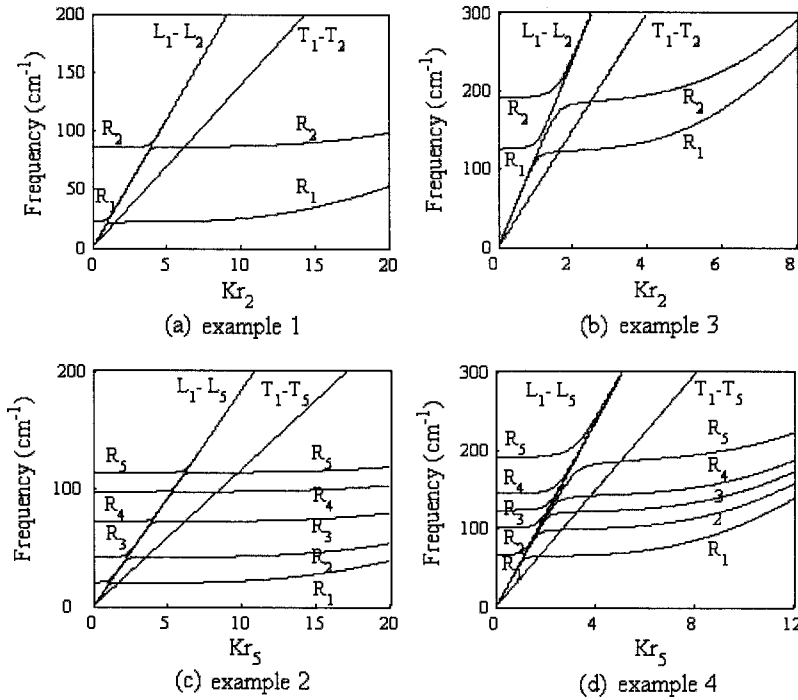


FIG. 3. Axisymmetric mode frequencies ( $n = 0$ ) of (a) example 1; (b) example 3; (c) example 2; and (d) example 4.

fore, two  $T$ -mode frequencies for the inner and outer tubes are almost indistinguishable.

Our results show that frequencies  $R_1$  and  $R_2$  in Fig. 3(a) for large-radius DWNT of example 1 are associated with an in-phase and a counterphase  $R$ -mode, respectively, while frequency  $R_1$  or  $R_2$  in Fig. 3(b) for small-radius DWNT of example 3, is basically associated with  $R$  mode of individual tube 2 or 1. Here, it should be mentioned that the RBM frequencies predicted by the present shell model for small-radius MWNTs are found to be in excellent agreement with experimental results<sup>19</sup> with relative errors less than 5% (see also Ref. 27).

In Fig. 3(a) and 3(b), the  $R$ -mode frequencies of the two DWNTs are usually insensitive to wave vector  $Kr_2$  when  $Kr_2 < 8$  or 4 (i.e., axial wavelength is relatively long) due to

negligible effect of bending stiffness, and approach the RBM frequencies as  $Kr_2$  goes to zero. For example, for example 3 (DWNT with inner radius 0.65 nm), it is seen from Fig. 3(b) that the two  $R$ -mode frequencies as  $K$  tends to zero are about 130 and 190  $\text{cm}^{-1}$ , respectively, in excellent agreement with MD simulation,<sup>17,26</sup> with relative errors less than 5%. The  $R$ -mode frequencies increase significantly with increasing  $Kr_2$  only in the range of  $Kr_2 > 8$  or 4 due to the strong effect of bending stiffness  $D$ . On the other hand, in the transition zone between  $R$ - and  $L$  modes where their frequencies are very close to each other,  $R$ - and  $L$  modes of the DWNTs are strongly coupled through the Poisson-ratio effect (because  $Kr_2 < 4$  and the effect of bending stiffness is negligible). In Fig. 3(b) for small-radius DWNT of example 3, this  $R$ - $L$  coupling (or transition) zone is relatively wide, especially for the higher-frequency  $R$  mode characterized by the radial vibration of the inner tube 1 of small radius. However, in Fig. 3(a) for large-radius DWNT of example 1, the  $R$ - $L$  coupling (or transition) zone is relatively wide only for the in-phase  $R$  mode of lower frequency  $R_1$  and almost vanishes for the counterphase  $R$  mode of higher frequency  $R_2$ . In other words, there is an abrupt transition between counterphase  $R$  mode and the  $L$  mode, and the  $R$ - $L$  coupling zone is very narrow and thus actually can be ignored. This unique feature of large-radius DWNT can be attributed to the dominant inter-layer vdW interaction associated with counterphase  $R$  mode of large-radius MWNTs. For large- and small-radius 5-wall CNTs, examples 2 and 4, qualitatively similar results are shown in Figs. 3(c) and 3(d), respectively.

### B. Axisymmetric longitudinal modes

First, it is seen from Figs. 3(a) and 3(b) for both large- and small-radius DWNTs, the two  $L$ -mode frequencies for  $n=0$  are almost indistinguishable, implying that  $L$  mode of one tube could be stimulated by  $L$  modes of adjacent tubes

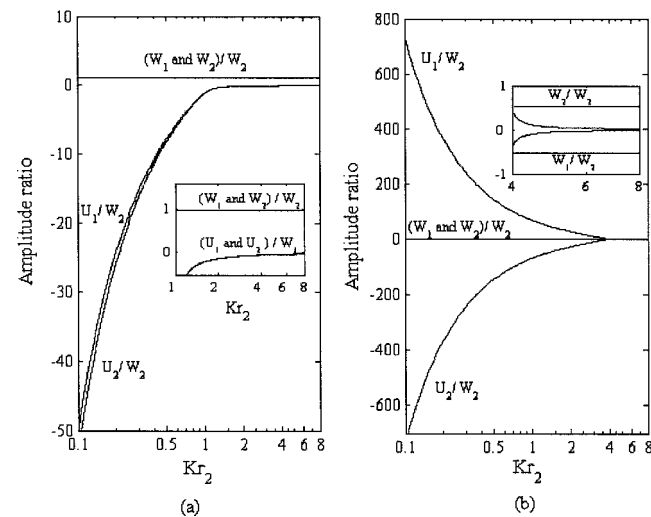


FIG. 4. Amplitude ratios associated with frequencies (a)  $L_1$  &  $R_1$  (inset) and (b)  $L_2$  &  $R_2$  (inset) shown in Fig. 3(a) for example 1.

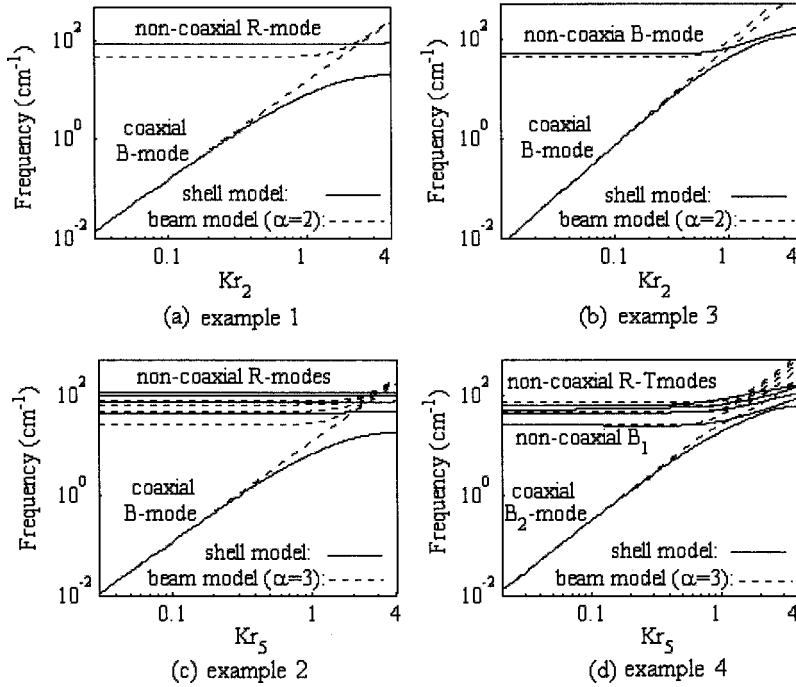


FIG. 5. Comparison between the multiple-beam model and the multiple-shell model when  $n=1$  for (a) coaxial  $B$  mode and noncoaxial  $R$  mode of example 1 ( $\alpha=2$ , Ref. 8); (b) coaxial and noncoaxial  $B$  modes of example 3 ( $\alpha=2$ , Ref. 8); (c) coaxial  $B$  mode and four noncoaxial  $R$  modes of example 2 ( $\alpha=3$ ); and (d) coaxial and noncoaxial  $B$  modes, and noncoaxial  $R$ - $T$  combined modes of example 4 ( $\alpha=3$ ).

through an even very weak coupling effect. Indeed, it is noted in Figs. 4(a) and 4(b) that, when  $Kr_2 < 4$  or 1, example 1 (DWNT) exhibits coupled axisymmetric  $L$  vibrations involving both tubes, among which the in-phase one [ $U_1 \approx U_2$ , see Fig. 4(a)] is associated with frequency  $L_1$  in Fig. 3(a), and the counterphase one [ $U_1 \approx -U_2$ ; see Fig. 4(b)] is associated with frequency  $L_2$  in Fig. 3(a). This phenomenon is in sharp contrast to the axisymmetric  $T$  modes and non-axisymmetric  $L$  modes (with larger  $n$ ) which are almost uncoupled vibrations of individual tubes.

In fact, it is known for elastic shells<sup>29</sup> that, when  $n=0$ , longitudinal vibration is always accompanied by a small but usually non-negligible radial vibration due to the  $R$ - $L$  coupling effect of Poisson ratio. Therefore, once an individual tube of the DWNT first vibrates in axisymmetric  $L$  mode, the associated  $R$  vibration induced by the Poisson-ratio effect could stimulate a small  $R$  vibration combined with a predominant  $L$  vibration of adjacent tubes through the interlayer vdW interaction. Here, almost identical  $L$ -mode frequencies of adjacent tubes are likely responsible for the strong coupling of axisymmetric  $L$  modes. For the same reasons, the strong coupling between  $L$  vibrations of individual tubes has also been observed for the small-radius DWNT, example 3 and the 5-wall CNTs, examples 2 and 4. Indeed, when the Poisson ratio  $\nu$  is set to zero, Eqs. (8) break into two systems for pure- $L$  vibrations of individual tubes and collective- $R$  vibrations of all individual tubes provided that  $Kr_N$  is small, say  $Kr_N < 8$  or 4 (i.e., axial wavelength is relatively long and thus the effect of bending stiffness is negligible). In particular, the resulting decoupled equations for individual tubes are radius independent. Thus, for MWNTs, coupling between  $L$  vibrations of concentric tubes is a result of the Poisson-ratio effect and the interlayer radial vdW interaction. This coupling effect becomes significant, especially when  $n=0$ , due to the fact that  $L$ -mode frequencies of individual tubes are almost identical when  $n=0$ . It is expected that the similar

concept can be used to explain the observed coupled resonant axisymmetric  $L$  modes of aligned SWNT ropes.<sup>11</sup>

#### IV. BEAMLIKE VIBRATION MODES OF MWNTs ( $n=1$ )

For MWNTs, noncoaxial vibrational modes are predicted based on a multiple-(Euler) beam model,<sup>8</sup> in which each nested tube of MWNTs is treated as an individual elastic (Euler) beam coupled with adjacent tubes through the interlayer vdW interaction. The intertube interaction per unit length along the axial direction is given by  $\alpha \times r(c\Delta w)$ , where  $\alpha r$  represents the intertube vdW interaction effective width between two adjacent tubes,  $r$  is the radius of inner tube,  $\Delta w$  is transverse deflection jump between the two tubes, and  $c$  is given by (3). In particular,  $\alpha=2$  is used in Ref. 8. In the present work, we shall compare the more accurate multiple-shell model with the multiple-beam model, to identify a better value of  $\alpha$  and further investigate beamlike modes, especially noncoaxial modes of MWNTs.

##### A. Large-radius MWNTs (the innermost radius 5 nm)

Let us start with the large-radius DWNT, example 1. Following the procedure demonstrated in Sec. II, six frequencies can be obtained for the DWNT with  $n=1$  and  $0 \leq Kr_2 \leq 4$ . For a comparison to the beam model<sup>8</sup> which gives two frequencies for a DWNT, the lowest frequency (corresponding to a beamlike bending mode) and the highest frequency  $R$  (of a radial mode) are identified from six frequencies and shown in Fig. 5(a), with associated amplitude ratios displayed in Figs. 6(a) and 6(b), respectively. As mentioned before, calculation of the amplitude ratios is essential for classifying all frequencies into  $L$ ,  $R$ ,  $T$ , or  $R$ - $L$  modes.

Beamlike bending of a shell is defined by  $n=1$  and  $w=u$ , where  $w$  and  $v$  represent radial and circumferential displacements of the shell, respectively. It is seen in Fig. 6(a) that,

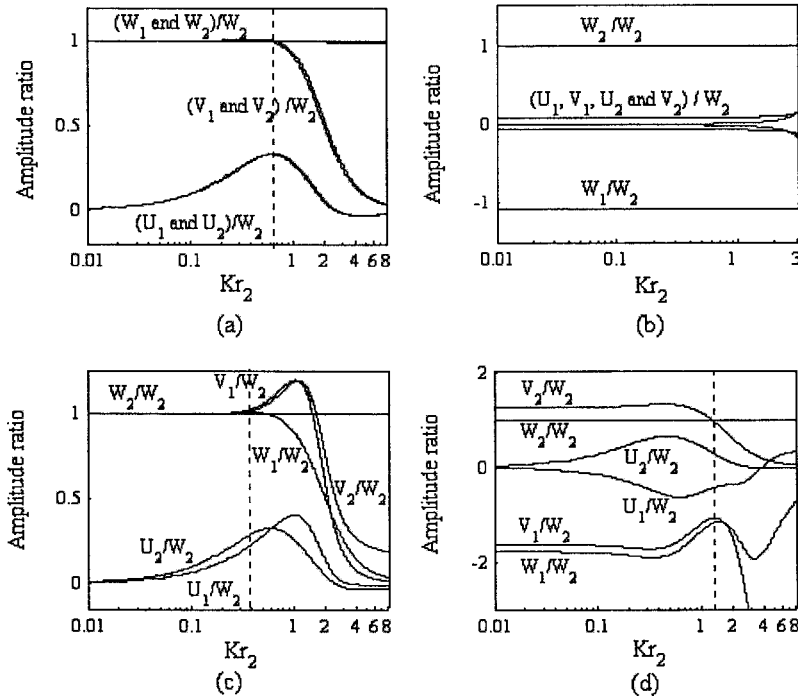


FIG. 6. Amplitude ratios associated with (a) frequency  $B$  and (b) frequency  $R$  shown in Fig. 5(a) for example 1, and (c) frequency  $B_1$  and (d) frequency  $B_2$  shown in Fig. 5(b) for example 3.

when  $Kr_2 > 2$ , the lowest frequency for  $n=1$  corresponds to an in-phase  $R$  mode of the DWNT having  $W_1 \approx W_2$  and  $(U_1, V_1, U_2, \text{ and } V_2) \ll W_2$ . The circumferential amplitudes  $V_1$  and  $V_2$  increase with decreasing wave vector  $Kr_2$ . When  $Kr_2$  is smaller than 1, we have  $W_1 = V_1 = V_2 = W_2$  and  $U_1 = U_2 \ll W_2$ , showing a coaxial bending ( $B$ ) mode characterized by a translation of the circular cross section. In Fig. 5(a), this frequency ( $B$ ) is compared to the coaxial mode frequency given by the beam model. As expected, when  $Kr_2 < 0.2$ , the beam model agrees very well with the shell model with relative errors less than 5%.

On the other hand, the amplitude ratios in Fig. 6(b) for the frequency  $R$  indicate  $W_1 \approx -W_2$  and  $(U_1, V_1, U_2, \text{ and } V_2) \ll W_2$ , which gives a non-coaxial  $R$ -mode with non-beam-like deformation of the cross section. In particular, this result ( $W_1 \approx -W_2$ ) predicted by the present shell model is the same as that predicted by the beam model for example 1. On the other hand, as seen from Fig. 5(a), the higher noncoaxial mode frequency obtained by the beam model with  $\alpha=2$  differs from frequency  $R$  given by the present shell model by around 50%. Similar results are obtained in Fig. 5(c) for coaxial  $B$  mode of the lowest frequency and four noncoaxial  $R$  modes of large-radius 5-wall CNT, example 2. The relative errors of the beam model with  $\alpha=3$  (which, as will be shown later, is more accurate than  $\alpha=2$ ) range from 30% to 50% for the four noncoaxial  $R$  modes. This discrepancy between the shell model and the (Euler) beam model is due to non-beamlike deformation of the cross section caused by the interlayer vdW interaction. This non-beamlike deformation is negligible for small-radius MWNTs, but could be significant for large-radius MWNTs due to their low radial rigidity. Therefore, consistent with our recent results (Ref. 34), the present work also suggests that the multiple-beam model is more accurate for small-radius MWNTs than large-radius MWNTs.

#### B. Small-radius MWNTs (the innermost radius 0.65 nm)

Next, let us consider small-radius MWNTs, example 3 (DWNT) and 4 (5-wall CNT). When  $n=1$ , the (lowest) two frequencies  $B_1$  and  $B_2$  of example 3, both of which correspond to beamlike bending modes, are identified from six frequencies and displayed in Fig. 5(b). The amplitude ratios associated with frequencies  $B_1$  and  $B_2$  are shown in Figs. 6(c) and 6(d), respectively.

We see from Fig. 6(c) that the lowest frequency  $B_1$  when  $Kr_2 < 0.5$  is associated with the coaxial beamlike  $B$  mode, while frequency  $B_2$  corresponds to  $W_1 \approx V_1 \approx -1.7W_2$  and  $W_2 \approx V_2$ , showing a noncoaxial  $B$  mode in which the inner and outer tubes are bent in opposite directions with individual circular cross sections. It is seen from Fig. 5(b) that, when  $Kr_2 < 0.3$ , the beam model<sup>8</sup> agrees well with the present shell model for both coaxial and noncoaxial  $B$  modes with relative errors less than 20% when  $\alpha=2$ . Our results showed that, for the noncoaxial  $B$  modes, the beam model with  $\alpha=3$  is in better agreement with the shell model with relative errors less than 10%. In particular,  $\alpha=3$ , selected by the best comparison to the shell model, is quite close to the value of  $\alpha=\pi$  obtained by a simple theoretical calculation (omitted here). Here, we mention that the noncoaxial mode and the associated frequency of small-radius DWNTs, predicted first by the beam model,<sup>8</sup> have been well confirmed by more recent atomistic simulation,<sup>20</sup> although relevant experimental data are not yet available.

For 5-wall CNT, example 4 (of the outermost radius 2 nm), similar results are obtained in Fig. 5(d). Accordingly, when  $Kr_5 < 0.3$ , the beam model with  $\alpha=3$  is adequate for both coaxial and noncoaxial  $B$  modes of small-radius MWNTs with relative errors less than 5% and for the three higher-order noncoaxial modes with relative errors less than 20%. Considering small-radius MWNTs, e.g., 3, 4, and 5-wall CNTs of the outermost radius 1.45, 1.65, and 1.9 nm,

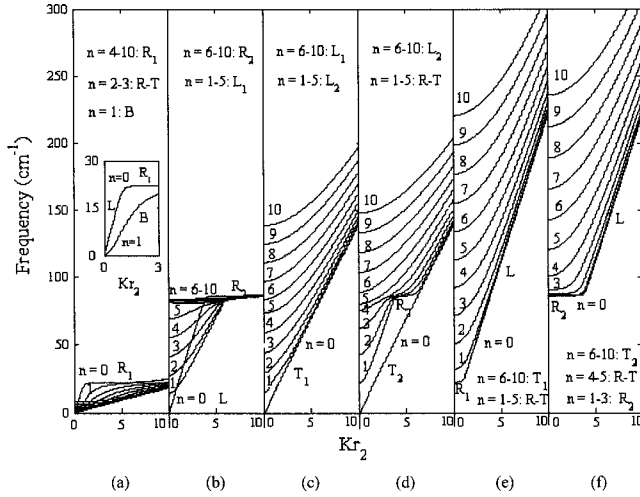


FIG. 7. Dependence of six frequencies on  $Kr_2$  for example 1. For a given  $n$  ( $n \geq 1$ ), the lowest frequency, the second lowest frequency, ..., and the highest frequency are shown in (a), (b), ..., and (f), respectively. ( $R$ : radial mode,  $L$ : longitudinal mode,  $T$ : torsional mode,  $B$ : bending mode, and  $R-T$ : radial and torsional combined mode).

we find that the beam model is in good agreement with the shell model for all coaxial and noncoaxial modes with maximum relative errors less than 10%. In these cases, due to high radial rigidity of small-radius individual tubes, all non-coaxial modes are associated with nearly beamlike bending modes with smaller cross-sectional deformation. Hence, the (Euler) beam model is relevant for MWNTs of smaller outermost radius (e.g., less than 2 nm).

## V. THE LOWEST FREQUENCY AND THE ASSOCIATED MODE

CNTs are expected to be the potential building blocks in nanodevices. Thus, the lowest frequency and the associated modes of CNTs are of practical interest. Here, based on the multiple-shell model, the lowest frequency and the associated modes are calculated for MWNTs.

First, let us consider double-wall nanotubes (DWNTs), example 1 and 3. The dependence of six frequencies on wave vector  $Kr_2$  are displayed in Figs. 7 and 8 for example 1 and 3, respectively, with  $0 \leq n \leq 10$  and  $0 \leq Kr_2 \leq 10$ . For a given  $n$  ( $n \geq 1$ ), the lowest frequency, the second lowest frequency, ..., and the highest frequency are presented in panels (a) to (f) of Figs. 7 and 8 for the two DWNTs. Notice that our results shown in Figs. 7 and 8 are consistent with those given in Ref. 15, which may be the only available published result for phonon dispersion relations of DWNTs, except that the acoustic transverse mode, i.e., coaxial bending mode given by the multiple-shell model for the two DWNTs has not been obtained in Ref. 15.

It is noted that, when the circumferential number  $n$  is sufficiently large, e.g.,  $n > 5$  for large-radius example 1 and  $n > 2$  for small-radius example 3, the two lowest frequencies  $R_1$  and  $R_2$ , shown in panels (a) and (b) of Figs. 7 and 8, are mainly associated with  $R$  modes, the highest two frequencies

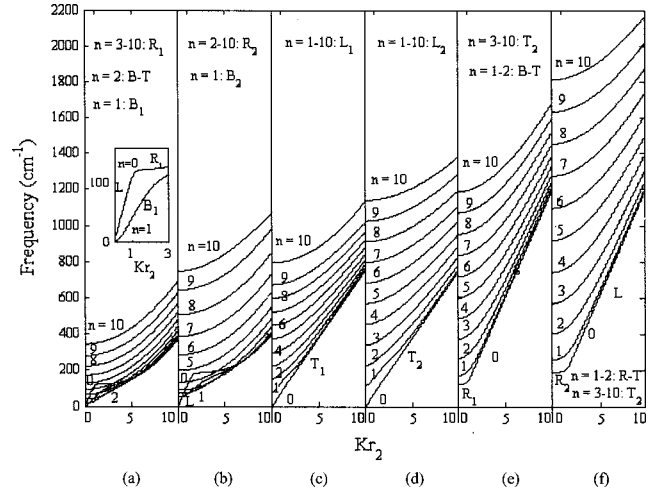


FIG. 8. Dependence of six frequencies on  $Kr_2$  for example 3. For a given  $n$  ( $n \geq 1$ ), the lowest frequency, the second lowest frequency, ..., and the highest frequency are shown in (a), (b), ..., and (f), respectively. ( $R$ : radial mode,  $L$ : longitudinal mode,  $T$ : torsional mode,  $B$ : bending mode, and  $R-T$ : radial and torsional combined mode).

$T_1$  and  $T_2$ , shown in panels (e) and (f) of Figs. 7 and 8, are primarily associated with  $T$  modes, while the two intermediate frequencies  $L_1$  and  $L_2$ , shown in panels (c) and (d) of Figs. 7 and 8 correspond to  $L$  modes of the two DWNTs. On the other hand, for given axial wave vector  $Kr_2$ , the lowest frequencies of the two DWNTs are represented by the envelope curves in Figs. 7(a) and 8(a), respectively. Obviously, the lowest frequency of the two DWNTs increases monotonically with increasing  $Kr_2 = \pi/[L/(r_2m)]$ , showing that, for any given ratio  $L/r_2$ , the lowest frequency of the two DWNT with simply supported ends always corresponds to the minimum axial half-wave number  $m=1$ .

Proceeding in the same way, analogous features are also obtained for large- and small-radius 5-wall CNTs, examples 2 and 4. Especially, the lowest frequency is also consistently associated with  $m=1$ . Here, the lowest frequency is plotted in Fig. 9 for all the  $N$ -wall CNTs considered here, as a function of the wave vector. It is clearly seen from Fig. 9 that, when  $Kr_N$  ( $N=2$  or  $5$ ) decrease from 8 to 0.05, the lowest frequencies of examples 1–4 decrease from the order of 10–100  $\text{cm}^{-1}$  to the order of 0.1  $\text{cm}^{-1}$ , and the associated modes shift from an in-phase  $R$  mode with relatively larger  $n$  ( $n=3-6$ ) to a combined  $R$ - and  $T$  mode with  $n=2-3$ , and finally, to a coaxial  $B$  mode with  $n=1$ .

## VI. CONCLUSIONS

A multiple-shell model is used to study axisymmetric vibration ( $n=0$ ) and beamlike vibration ( $n=1$ ) of MWNTs. An updated value of the bending stiffness for SWNTs is suggested based on recent data in the literature, which leads to good agreement of the present shell model with atomistic model for phonon-dispersion relations of SWNTs. The main results of the present work are summarized as follows.

(1) In axisymmetric vibration ( $n=0$ ),  $L$ - and  $R$  modes are

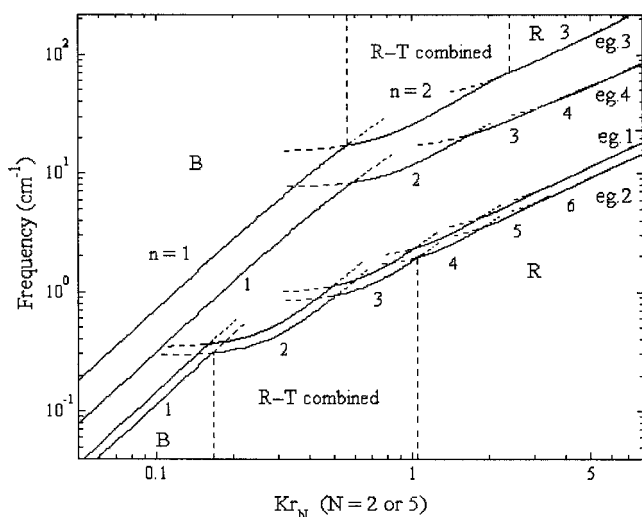


FIG. 9. The lowest frequency and associated modes for examples 1 to 4.

strongly coupled with each other in a transition zone between the two modes due to the Poisson-ratio effect. In addition, different from nonaxisymmetric  $L$  modes (with larger  $n$ ) of MWNTs, which are basically uncoupled longitudinal vibrations of individual tubes, axisymmetric  $L$  modes of MWNTs are usually collective vibrations of nested tubes for larger axial wavelength-to-diameter ratios. In particular, the present shell model shows that this coupling effect becomes significant only when  $n=0$  because of almost identical  $L$ -mode frequencies of individual tubes. This interesting phenomenon of MWNTs predicted by the present model would not be easily studied by other methods.

(2) For beamlike vibration ( $n=1$ ), the multiple-(Euler)

beam model is found to be in good agreement with the more accurate multiple-shell model for almost coaxial  $B$  mode of both large- and small-radius MWNTs and the noncoaxial  $B$  modes of small-radius MWNTs (e.g., 2–5 wall CNTs of outermost radius less than 2 nm), with relative errors less than 10%. However, the relative errors between the two models are up to 30% to 50% for high-order noncoaxial modes of large-radius MWNTs, due to significant non-beamlike cross-sectional deformation caused by the interlayer vdW interaction. Therefore, the multiple-beam model is more relevant for small-radius MWNTs than large-radius MWNTs. These results offer a detailed comparison between the shell model and the beam model for MWNTs with clear conclusions.

(3) The lowest frequency of MWNTs simply supported at both ends is always associated with the minimum axial half-wave number  $m=1$ . In this case, when the length-to-outermost radius ratio ( $L/r_N$ ) increases or the normalized wave vector ( $Kr_N$ ) decreases, the lowest frequency of MWNTs decreases monotonically and the associated mode shifts from a  $R$  mode with larger  $n$  (say,  $n=3-6$ ), to an  $R-T$  combined mode with smaller  $n$  (say,  $n=2-3$ ), and finally, to a beamlike coaxial  $B$  mode with  $n=1$ . The critical value of the length-to-outermost radius ratio for the lowest frequency to be a beamlike coaxial  $B$  mode is about 6 for small-radius MWNTs, and 20 for large-radius MWNTs. These results, which remain absent in the literature, could find significant application to the design of MWNTs-based devices.

#### ACKNOWLEDGMENT

The financial support of the Natural Science and Engineering Research Council of Canada (NSERC) is gratefully acknowledged.

\*Electronic address: c.ru@ualberta.ca

- <sup>1</sup>A. Jorio, M. A. Pimenta, A. G. Souza Filho, R. Saito, G. Dresselhaus, and M. S. Dresselhaus, *New J. Phys.* **5**, 139.1 (2003).
- <sup>2</sup>R. A. Jishi, L. Venkataura, M. S. Dresselhaus, and G. Dresselhaus, *Chem. Phys. Lett.* **209**, 77 (1993).
- <sup>3</sup>J. Yu, R. K. Kalia, and P. Vashishta, *J. Chem. Phys.* **103**, 6697 (1995).
- <sup>4</sup>R. Saito, T. Takeya, T. Kimura, G. Dresselhaus, and M. S. Dresselhaus, *Phys. Rev. B* **57**, 4145 (1998).
- <sup>5</sup>V. N. Popov, V. E. Van Doren, and M. Balkanski, *Phys. Rev. B* **61**, 3078 (2000).
- <sup>6</sup>D. Sanchez-Portal, E. Artacho, J. M. Soler, A. Rubio, and P. Ordejon, *Phys. Rev. B* **59**, 12678 (1999).
- <sup>7</sup>K. Sohlberg, B. G. Sumpter, R. E. Tuzun, and D. W. Noid, *Nanotechnology* **9**, 30 (1998).
- <sup>8</sup>J. Yoon, C. Q. Ru, and A. Mioduchowski, *Phys. Rev. B* **66**, 233402 (2002).
- <sup>9</sup>D. Kahn and K. W. Kim, *J. Appl. Phys.* **89**, 5107 (2001).
- <sup>10</sup>A. Raichura, M. Dutta, and M. A. Stroschio, *J. Appl. Phys.* **94**, 4060 (2003).
- <sup>11</sup>C. E. Bottani, A. Li Bassi, M. G. Beghi, A. Podesta, P. Milani, A. Zakhidov, R. Baughman, D. A. Walters, and R. E. Smalley,

*Phys. Rev. B* **67**, 155407 (2003).

- <sup>12</sup>G. D. Mahan, *Phys. Rev. B* **65**, 235402 (2002).
- <sup>13</sup>H. Suzuura and T. Ando, *Phys. Rev. B* **65**, 235412 (2002).
- <sup>14</sup>L. Chico and R. Perez-Alvarez, *Phys. Rev. B* **69**, 035419 (2004).
- <sup>15</sup>M. G. Xia, S. L. Zhang, E. H. Zhang, S. M. Zhao, and X. J. Zuo, *Phys. Rev. B* **69**, 233407 (2004).
- <sup>16</sup>M. G. Xia, S. L. Zhang, X. J. Zuo, E. H. Zhang, S. M. Zhao, J. Li, L. Zhang, Y. C. Liu, and R. Liang, *Phys. Rev. B* **70**, 205428 (2004).
- <sup>17</sup>V. N. Popov and L. Henrard, *Phys. Rev. B* **65**, 235415 (2002).
- <sup>18</sup>J. M. Benoit, J. P. Buisson, O. Chauvet, C. Godon and S. Lefrant, *Phys. Rev. B* **66**, 073417 (2002).
- <sup>19</sup>X. L. Zhao, Y. Ando, L. C. Qin, H. Kataura, Y. Maniwa, and R. Saito, *Chem. Phys. Lett.* **361**, 169 (2002).
- <sup>20</sup>C. Y. Li and T. W. Chou, *Appl. Phys. Lett.* **84**, 121 (2004).
- <sup>21</sup>C. Q. Ru, *Phys. Rev. B* **62**, 9973 (2000).
- <sup>22</sup>C. Q. Ru, *J. Appl. Phys.* **89**, 3426 (2001).
- <sup>23</sup>C. Q. Ru, "Elastic models for carbon nanotubes," in *Encyclopedia of Nanoscience and Nanotechnology*, (edited by H. S. Nalwa) (American Scientific Publishers, 2004), Vol. 2, pp. 731–744.
- <sup>24</sup>C. Y. Wang, C. Q. Ru, and A. Mioduchowski, *J. Nanosci. Nanotechnol.* **3**, 199 (2003).

- <sup>25</sup>C. Y. Wang, C. Q. Ru, and A. Mioduchowski, *Int. J. Solids Struct.* **40**, 3893 (2003).
- <sup>26</sup>C. Y. Wang, C. Q. Ru, and A. Mioduchowski, *J. Appl. Mech.* **71**, 622 (2004).
- <sup>27</sup>C. Y. Wang, C. Q. Ru, and A. Mioduchowski, *J. Appl. Phys.* **97**, 024310 (2005).
- <sup>28</sup>W. Flugge, *Stresses in Shells* (Springer-Verlag, Berlin, 1960).
- <sup>29</sup>S. Markus, *The Mechanics of Vibration of Cylindrical Shells* (Elsevier, Amsterdam, 1988).
- <sup>30</sup>B. I. Yakobson, C. J. Brabec, and J. Bernholc, *Phys. Rev. Lett.* **76**, 2511 (1996).
- <sup>31</sup>D. H. Robertson, D. W. Brenner, and J. W. Mintmire, *Phys. Rev. B* **45**, 12592(R) (1992).
- <sup>32</sup>K. N. Kudin, G. E. Scuseria, and B. I. Yakobson, *Phys. Rev. B* **64**, 235406 (2001).
- <sup>33</sup>O. Gulseren, T. Yildirim, and S. Ciraci, *Phys. Rev. B* **65**, 153405 (2002).
- <sup>34</sup>J. Yoon, C. Q. Ru, and A. Mioduchowski, *Composites, Part B* **35**, 87 (2004).